

# Particle-in-cell simulations of electron transport from plasma turbulence: recent progress in gyrokinetic particle simulations of turbulent plasmas

Z Lin<sup>1</sup>, G Rewoldt<sup>2</sup>, S Ethier<sup>2</sup>, T S Hahm<sup>2</sup>, W W Lee<sup>2</sup>, J L V Lewandowski<sup>2</sup>, Y Nishimura<sup>1</sup>, and W X Wang<sup>2</sup>

<sup>1</sup> University of California, Irvine, California 92697 USA

<sup>2</sup> Princeton Plasma Physics Laboratory, Princeton, New Jersey 08543 USA

E-mail: rewoldt@pppl.gov

**Abstract.** Recent progress in gyrokinetic particle-in-cell simulations of turbulent plasmas using the gyrokinetic toroidal code (GTC) is surveyed. In particular, recent results for electron temperature gradient (ETG) modes and their resulting transport are presented. Also, turbulence spreading, and the effects of the parallel nonlinearity, are described. The GTC code has also been generalized for non-circular plasma cross-section, and initial results are presented. In addition, two distinct methods of generalizing the GTC code to be electromagnetic are described, along with preliminary results. Finally, a related code, GTC-Neo, for calculating neoclassical fluxes, electric fields, and velocities, are described.

## 1. Introduction

The gyrokinetic toroidal code (GTC) [1] is a particle-in-cell (PIC) simulation code in radially-global toroidal geometry for solving the linear or nonlinear gyrokinetic equation. As a PIC code, it employs efficient sampling of the five-dimensional (5D) phase space (*i.e.*, three spatial dimensions, energy, and pitch angle, since the gyrokinetic equation is already averaged over the gyrophase angle). The GTC code uses a global equilibrium-magnetic-field-aligned mesh that respects the physical periodicity of the toroidal geometry in the toroidal and poloidal angles. This is illustrated in the linear regime in Fig. 1, where the perturbed electrostatic potential value is represented by the colors, and the constant potential lines closely follow the equilibrium magnetic field lines, drawn as narrow black lines.

This mesh is efficient for the calculation of linear toroidal eigenmodes, and also nonlinearly; it reduces the number of computations by of order  $(a/\rho)^2$ , where  $a$  is the boundary minor radius and  $\rho$  is the gyroradius of the non-adiabatic plasma species. For realistic cases, this can mean a reduction by of order  $n \sim 10^3$ , where  $n$  is the toroidal mode number. The GTC code is designed for massively parallel computing, which is needed to simulate reactor-scale plasmas, and it can keep all toroidal mode numbers (harmonics) up to of order  $n \sim 10^3$ .

The present standard version of GTC uses a model toroidal magnetic geometry with circular-cross-section, concentric magnetic surfaces, and works in the electrostatic limit, but efforts are under way to generalize it to non-circular, non-concentric magnetic surfaces, and, by two complementary approaches, to include electromagnetic effects; these efforts will be described here, and preliminary results will be shown.

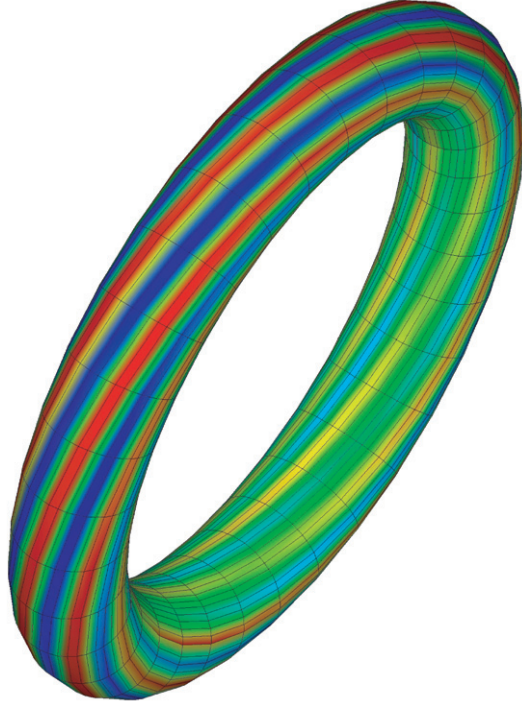


**Figure 1.** GTC mesh for a single magnetic surface, showing equilibrium magnetic field lines (black), and values of perturbed electrostatic potential in linear regime (colors).

## 2. Benchmarking

The GTC code can now include contributions from the non-adiabatic responses of both electrons and ions. When both are included in the calculation in the linearized mode of operation, it can obtain linear growth rates for both the ion temperature gradient (ITG) mode and the trapped-electron mode (TEM), and we refer to an ITG root and a TEM root. These eigenfrequencies have been compared, for standard Cyclone parameters [2], with those obtained from the comparable global code GT3D [3], and with those obtained from the radially-local eigenvalue code FULL [4, 5]. For this comparison, all three codes use the same density and temperature values and gradients at the reference magnetic surface,  $r/a = 0.5$ , but the FULL code only knows about the temperature and density gradients on that surface, the GTC code uses fixed values but varying gradients away from that surface, and the GT3D code uses both varying values and varying gradients away from that surface; also, GTC and GT3D use different algebraic forms for the variation of the density and temperature gradients. Varying the ion temperature gradient parameter  $R/L_{T_i}$  (where  $R$  is the toroidal major radius and  $L_{T_j}$  is the temperature gradient scale length for species  $j$ ) (or  $\eta_i \equiv (d \ln T_i / dr) / (d \ln n / dr)$ ), at fixed electron temperature gradient parameter  $R/L_{T_e} = 6.92$ , fixed density gradient parameter  $R/L_n = 2.22$  (where  $L_n$  is the electron and ion density gradient scale length), and fixed  $k_\theta \rho_i = 0.335$ , (all values are on the reference surface), gives the linear growth rate and real frequency variation shown in Fig. 2.

As an eigenvalue code, the FULL code can track the TEM root and the ITG root separately, but as initial-value codes, GTC and GT3D always track the most unstable root. Thus, where the growth rate curves cross, the GTC and GT3D codes jump from the TEM root to the ITG root, and the real frequencies take a corresponding jump. The three codes show good agreement for linear growth rates, and acceptable agreement for the real frequencies. Nonlinear runs of GTC with trapped electrons, for convergence studies and for planned benchmarking against GT3D,

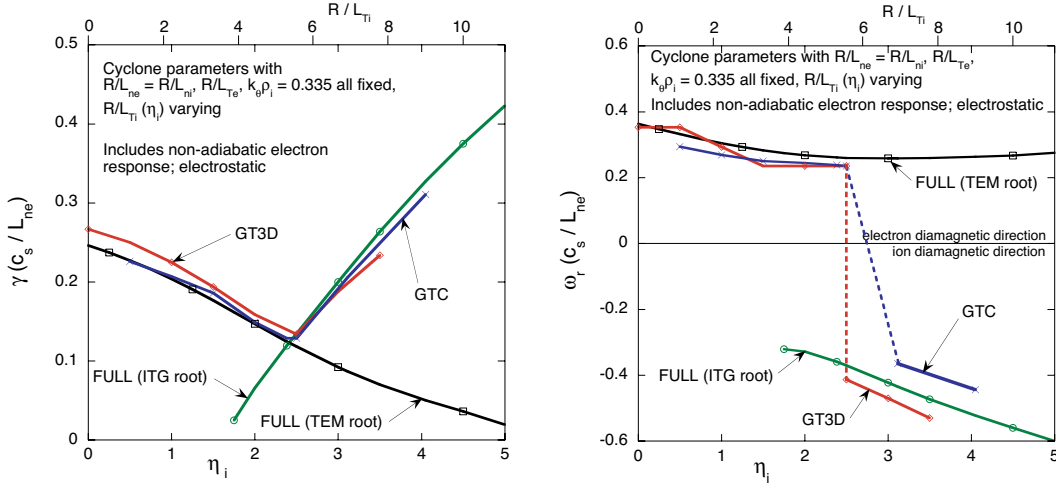


**Figure 2.** Linear frequency comparison for GTC, GT3D, and FULL, from  $R/L_{Ti}$  ( $\eta_i$ ) scan with trapped electrons.

are now under way.

### 3. Electron Temperature Gradient Modes

Very-high- $n$  electron temperature gradient modes, with  $k_{\theta}\rho_e \sim 1$ , have been calculated with the GTC code [6] in the limit of adiabatic ion response. These calculations are radially-global, in a wide toroidal annulus, thereby avoiding the limitations of previous flux-tube type calculations with periodic radial boundary conditions. For a time  $t = 20/\gamma_0$  after saturation, where  $\gamma_0$  is the linear growth rate, a poloidal contour plot of the electrostatic potential is shown in Fig. 3. The poloidal projection of a typical electron orbit from saturation to  $t$  is also shown. The length unit is  $\rho_e$ .

The radially-elongated “streamers” in the electrostatic potential, on the large major-radius side, scale in length with the device size. The eddy turnover time  $\tau \sim 16/\gamma_0$ , so that the nonlinear decorrelation rate  $\gamma_{nl} \ll \gamma_0$ . Note that the electron orbit does not rotate with the streamers, and in fact remains quite narrow, thus limiting the electron energy transport to far less than that implied by the radial correlation length of the streamers. The transport here is driven by the wave-particle interaction, and the usual mixing-length estimates for it are quite inaccurate. The observed transport level here is substantially less than that seen in some previous simulations for ETG modes, and this is an area of ongoing research.

The nonlinear saturation mechanism for the ETG modes seen in the GTC results is nonlinear toroidal couplings, which regulate the ETG turbulence level. This process is illustrated in Fig. 4. In a special GTC run designed to illustrate this nonlinear saturation process, only two toroidal mode numbers in the linearly unstable range,  $n_1 = 95$  and  $n_2 = 110$ , are allowed to grow until they have reached large amplitude; then all toroidal mode numbers are allowed to grow. The first step is the generation of a low- $n$  (linearly stable) quasi-mode with  $n = \Delta n = 15$ , by the coupling condition  $(n_1, m_1) + (n_2, m_2) \implies (\Delta n, \Delta m) = (n_2 - n_1, m_2 - m_1)$ , where  $m_j = qn_j$  is the corresponding poloidal harmonic number. The quasi-mode will be on the “meso-scale”, with an optimum mode number  $\Delta n \sim \sqrt{n_1}$ , and will have no significant ballooning structure, with wavelength along the magnetic field line  $\lambda_{\parallel} \sim qR\sqrt{n_1}$ . In the second step, energy is transferred to the nonlinear mode ( $n = 80$  in this example) by  $(n_1, m_1) + (\Delta n, \Delta m) \implies (n_1 - \Delta n, m_1 - \Delta m)$ , and streamers are nonlinearly generated. This process continues, filling in toroidal mode numbers

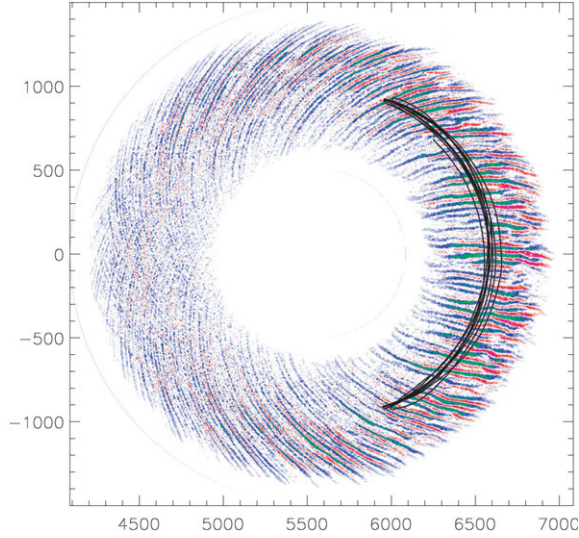


**Figure 3.** Electrostatic potential and typical electron orbit for ETG mode.

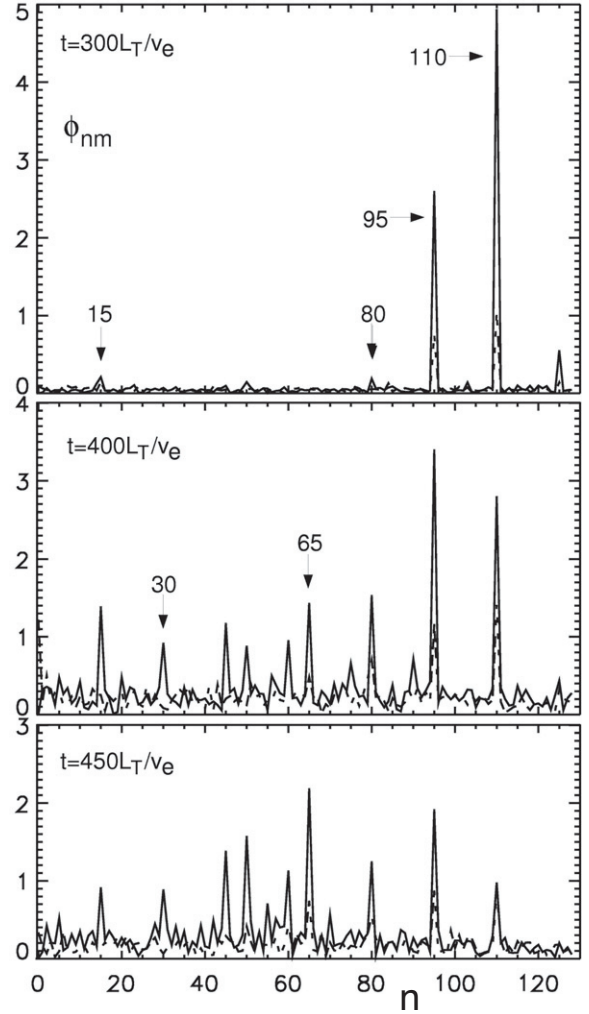


**Figure 4.** Toroidal mode number  $n$  spectra before and after saturation of the pump modes, at  $r/a = 0.5$ .

all the way down to the quasi-mode. The spectral transfer that is facilitated by the quasi-mode is nonlocal in  $n$ -space, and constitutes a kind of “Compton scattering”. The streamer coupling is a toroidal-geometry specific effect. However, to recover this spectral transfer computationally, it is necessary to retain all toroidal mode numbers, and there will then be sufficient channels for the transfer.

#### 4. Parallel Nonlinearity

In the nonlinear gyrokinetic equation, it has generally been the practice to include only the  $\mathbf{E} \times \mathbf{B}$  nonlinearity, and not the parallel nonlinearity corresponding to the  $((q_j/m_j)E_{\parallel}(\partial\delta f_j/\partial v_{\parallel}))$  term, even though this term is needed to prove energy conservation for this equation. The GTC code has always contained the parallel nonlinearity, but it has not been switched on until now. For a standard Cyclone case [2], inclusion of the additional nonlinearity accelerates the approach to the saturated level of ion energy transport, possibly by providing an additional channel to reach a steady state. This is illustrated in Fig. 5, for a case with standard Cyclone parameters

and adiabatic electron response. Also, the saturated level of ion energy transport is lower, and the saturated level of zonal flow (the  $n = 0, m = 0$  mode) is higher due to this additional nonlinearity, as shown in Fig. 6. It may possibly also cause a different pattern of (test particle) diffusion, and even a different transport scaling. Additional investigation of these effects is planned.

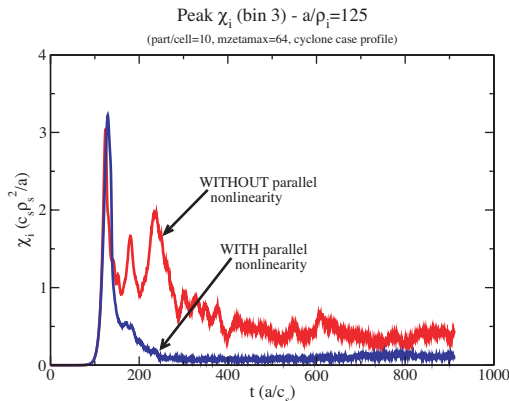


**Figure 5.** Time history of thermal diffusivity, without and with parallel nonlinearity term.

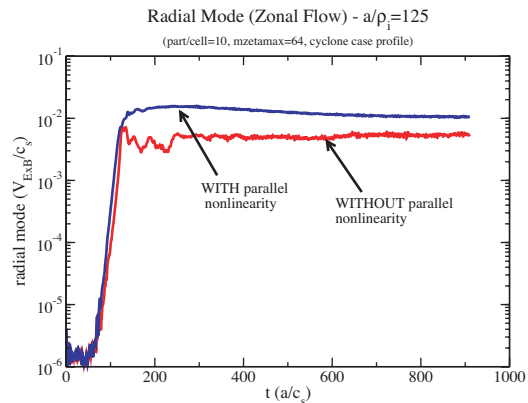


**Figure 6.** Time history of zonal flow, without and with parallel nonlinearity term.

## 5. Turbulence Spreading from Edge to Stable Core

The GTC code has been used to simulate the process of ITG turbulence spreading from a strongly unstable “edge” region to an effectively stable (due to the so-called Dimits shift effect [2]) “core” region. This particular GTC simulation has  $R/L_{Ti} = 10.6$  in the edge region, but  $R/L_{Ti} = 5.3$  in the core region, as shown in Fig. 7 (a). The turbulence intensity grows only in the unstable edge region at earlier times, but spreads into the stable core region at later times, as shown in Fig. 7. Further details of this are given in Ref. [7].

## 6. Gyrokinetic Simulation of Microturbulence for Shaped Plasmas

A version of GTC has been developed with a number of generalized and extended features. These include experimentally realistic input density and temperature profiles, interfacing to numerically-calculated MHD equilibria, allowing non-circular and non-concentric magnetic surfaces, with an accurate gyrotransformation, systematic treatment of plasma rotation and sheared  $\mathbf{E} \times \mathbf{B}$  flow (calculated in GTC-Neo, to be discussed below), and a nonuniform mesh in correlation with the local gyroradius. The current version of this general-geometry GTC is electrostatic; it has been tested for adiabatic electron response, but remains to be tested with trapped-electron response via a higher-order correction. Initial results for the ITG mode electrostatic potential for a shaped cross-section case are shown in Fig. 8. A comparison of the steady-state zonal flow between the new general-geometry version of GTC, for a circular-cross-section case, and the original GTC with model circular geometry, is shown in Fig. 9, with reasonably good agreement. Further details for the general-geometry GTC are given in Ref. [8].

## 7. Electromagnetic Effects in Massless Electron Limit

Two alternative approaches to extending the GTC code to be electromagnetic, for application to finite- $\beta$  plasmas, are being pursued. In this section, work on a method employing a fluid-

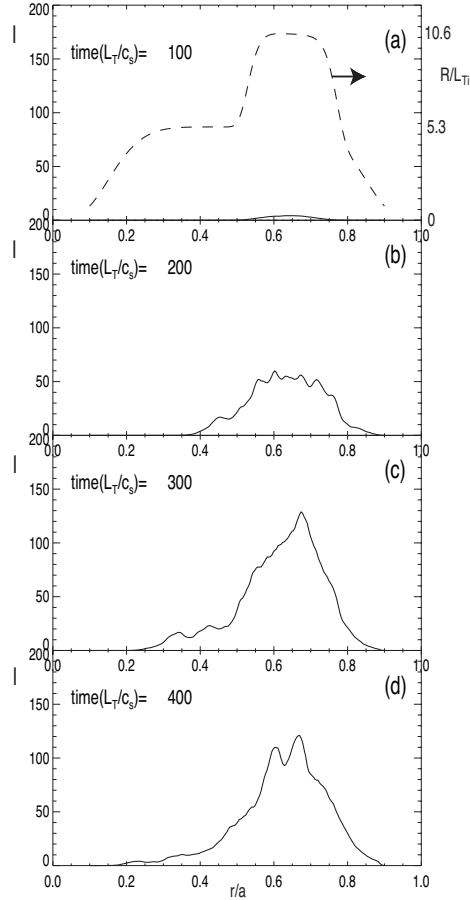


**Figure 7.** Spatio-temporal evolution of turbulence intensity from GTC simulation.

kinetic electron hybrid model [9], with an electron-ion mass-ratio expansion, is described. In the next section, work on a method using the split-weight scheme [10] is described. Electromagnetic effects are necessary in order to study modes such as the Alfvén ITG mode (or kinetic ballooning mode), which are unstable at sufficiently high  $\beta$ , and also toroidal Alfvén eigenmodes (TAEs), which can be destabilized by energetic particles. In the hybrid method, at lowest order the electrons are massless, and can be solved as a fluid; at higher order the solution is kinetic. A new finite-element-method elliptic solver for the field equations has been developed as part of this work. Initial results from a linear electromagnetic calculation of the ITG mode in the massless electron limit are shown for the perturbed electrostatic potential in Fig. 10, and for the component of the perturbed vector potential along the equilibrium magnetic field lines in Fig. 11.

## 8. Electromagnetic Effects via Split-Weight Scheme

In this approach, the split-weight scheme [10] is used for toroidal, kinetic PIC simulations with kinetic electrons. The scheme removes the adiabatic electron response analytically, and then solves for the non-adiabatic electron response numerically. The current implementation is electrostatic, but will be made electromagnetic, solving the gyrokinetic Poisson equation and Ampère’s law. Previous 1D simulations with the split-weight scheme showed: (1) more accurate linear growth rates, (2) a cleaner power spectrum, and (3) better conservation properties even

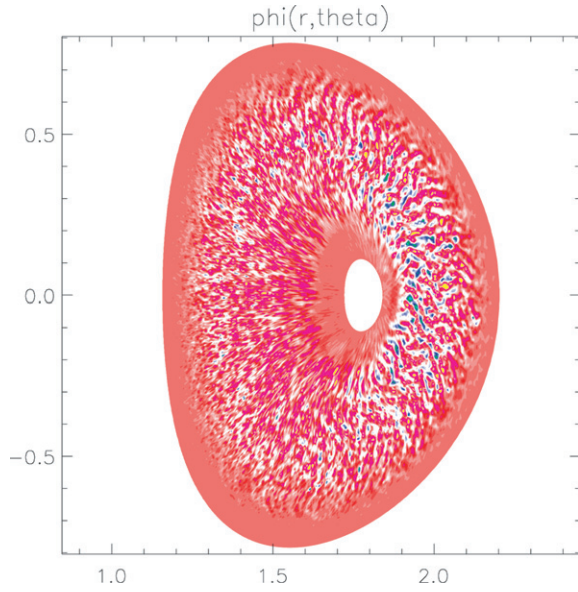


**Figure 8.** Poloidal cross-section of perturbed electrostatic potential for shaped plasma cross-section.

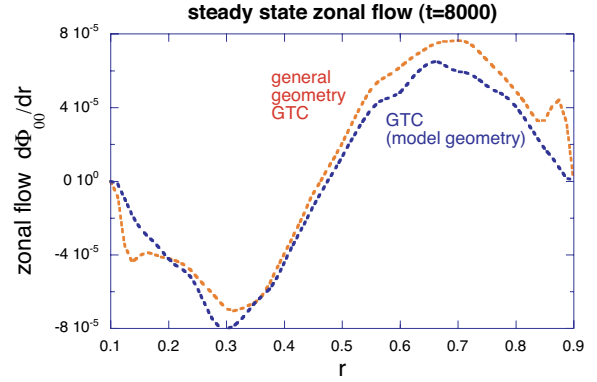


**Figure 9.** Radial variation of zonal flow.

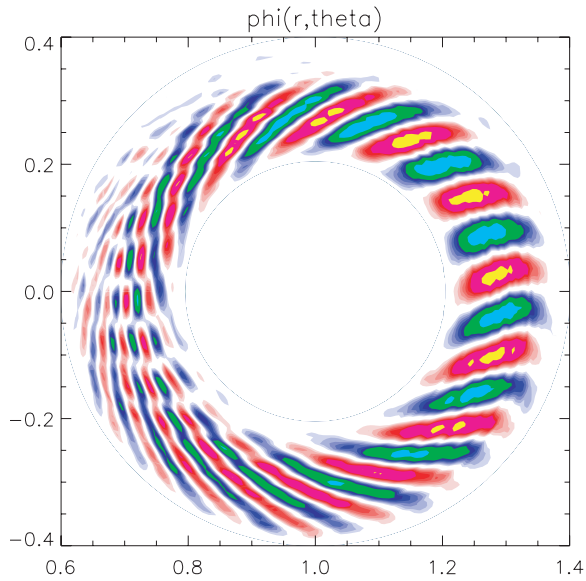


**Figure 10.** Poloidal cross-section of perturbed electrostatic potential.

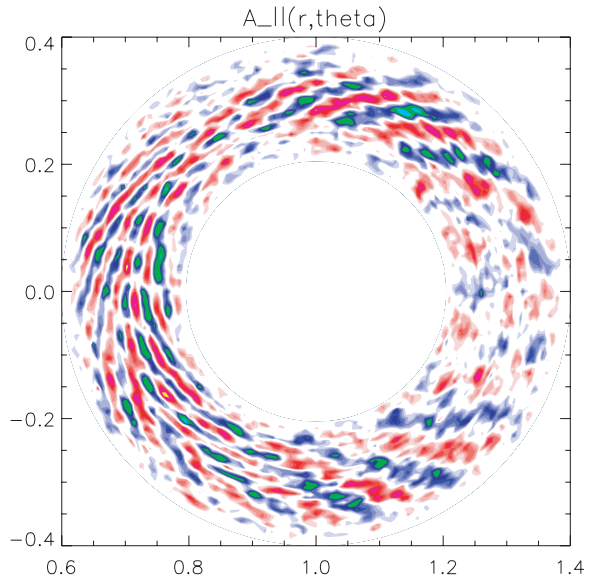


**Figure 11.** Poloidal cross-section of perturbed parallel vector potential.

for few electron markers,  $N_e \ll N_i$ , compared to other methods. The nonlinear splitting scheme for toroidal plasmas takes  $F_e = F_M \exp(e\Phi/T_e) + h$ , and solves for the non-adiabatic electron weight  $w = h/F_e$ . Using this split-weight scheme, for the non-adiabatic electron response only, allows for calculation of the turbulent and collisional friction between magnetically trapped and untrapped electrons. The current density and other scalar quantities are deposited on a structured, but not logically rectangular grid, as illustrated in Fig. 12, every timestep, and inversion of the field equations is carried out using a finite-element method with triangular

elements. A corresponding finite-element Poisson solver is used to invert equations of the form  $A\partial\Phi/\partial t = S$  (for 32 or 64 different stiffness matrices  $A$ , on different poloidal planes). Initial results for the electrostatic potential from this approach are shown in Fig. 13.

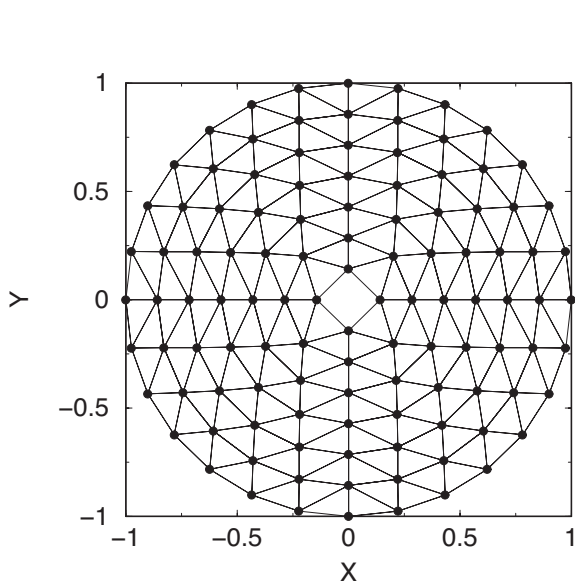


**Figure 12.** Triangular finite-element grid.

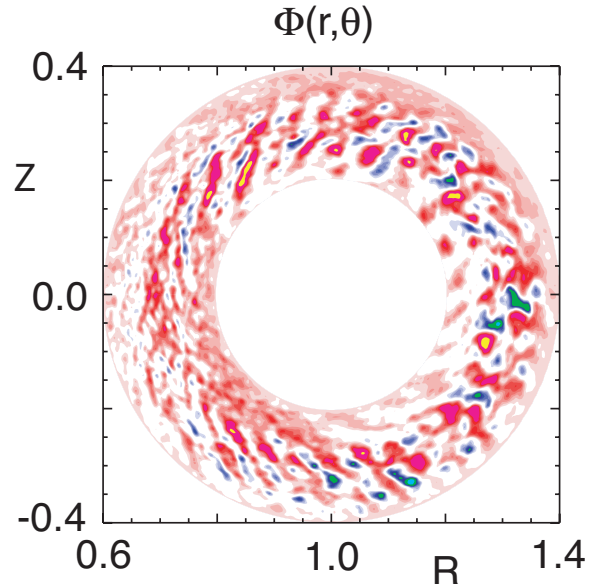


**Figure 13.** Poloidal cross-section of electrostatic potential.

### 9. Neoclassical Transport Calculation: GTC-Neo

The global particle code GTC-Neo [11] calculates neoclassical (nonturbulent collisional, for toroidal geometry) fluxes of particles, momentum, and energy, as well as associated quantities such as the radial electric field, the bootstrap current, and the poloidal velocity. The calculation is intrinsically nonlocal over the radial scale length of the ion banana width, due to the included finite orbit-size effects; this normally implies radial smoothing of the results. The GTC-Neo code has been interfaced with numerical MHD equilibrium codes for shaped (noncircular cross section) geometry, and with an experimental data analysis code for access to input profiles of density, temperature, and toroidal rotation velocity. The code currently includes only a single ion species, but it will be generalized in the future to multiple ion species, so that impurity and hot beam species, for instance, can be included. The GTC-Neo code currently runs on a massively-parallel IBM-SP computer. A number of experimental cases have now been run for the NSTX spherical torus. Results from GTC-Neo for an illustrative discharge, in comparison to experimental results and to standard (radially local) neoclassical results, are shown, for the input ion temperature profile in Fig. 14, for the ion heat flux in Fig. 15 and for the radial electric field in Fig. 16. For this case, the GTC-Neo ion heat flux profile is closer to the experimental profile than is the standard neoclassical profile, and also smoother. For this case, the radial electric field profile is relatively close to the standard neoclassical profile, but other discharges display larger differences.

### 10. Conclusions

Progress is occurring on many fronts now for the GTC code. The standard version now of the GTC code works in the electrostatic limit, with circular concentric magnetic surfaces,

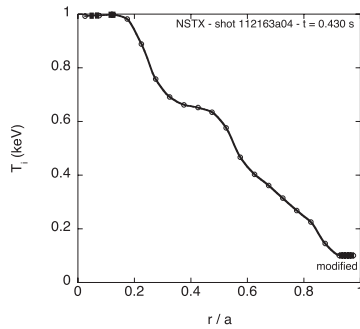


**Figure 14.** Radial profile of (input) ion temperature.

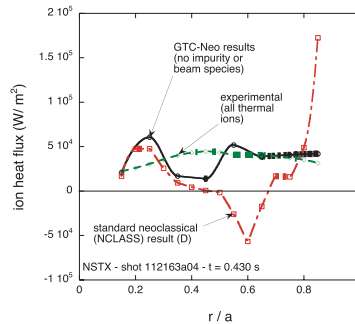


**Figure 15.** Radial profiles of ion heat flux.

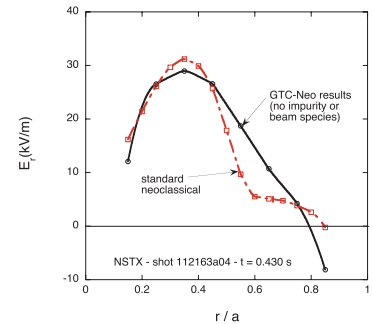


**Figure 16.** Radial profiles of radial electric field.

and includes trapped electrons. It is producing physics results, such as: linear and nonlinear benchmarking, ETG modes, effects of parallel nonlinearity, and turbulence spreading. The generalization of GTC for general geometry, with non-circular, non-concentric cross-section, is beginning to produce results. Two complementary approaches to the electromagnetic generalization of GTC are being investigated. Also, the related code GTC-Neo is being used to calculate neoclassical fluxes and radial electric fields for experimental cases for NSTX. However, the challenge will be to put all of these extensions of GTC together into a single unified version of the code.

### Acknowledgments

This work was supported by the Center for Gyrokinetic Particle Simulation of Turbulent Transport in Burning Plasmas under the SciDAC program of the US Department of Energy, and by DOE Cooperation Agreement No. DE-FC02-04ER54796 (UCI) and DOE Contract No. DE-AC02-76-CHO-3073 (PPPL).

### References

- [1] Lin Z, Hahm T S, Lee W W, Tang W M, and White R B 1998 *Science* **281** 1835
- [2] Dimits A M, *et al.* 2000 *Phys. Plasmas* **7** 969
- [3] Idomura Y, Tokuda S, and Kishimoto Y *Nucl. Fusion* **43** 234
- [4] Rewoldt G, Tang W M, and Chance M S 1982 *Phys. Fluids* **25** 480
- [5] Rewoldt G, Tang W M, and Hastie R J 1987 *Phys. Fluids* **30** 807
- [6] Lin Z, Chen L, and Zonca F 2005 *Phys. Plasmas* **12** 056125
- [7] Hahm T S, Diamond P H, Lin Z, Rewoldt G, Gurcan O, and Ethier S 2005 “On the dynamics of edge-core coupling” *Phys. Plasmas* **12** in press
- [8] Wang W 2005 “New Insights from General Geometry Simulations of Plasma Transport”, *Proc. SciDAC Conf. (San Francisco, June 26–30)*
- [9] Lin Z and Chen L 2001 *Phys. Plasmas* **8** 1447
- [10] Lee W W, Lewandowski J L V, Hahm T S, and Lin Z 2001 *Phys. Plasmas* **8** 4435
- [11] Wang W X, Tang W M, Hinton F L, Zakharov L E, White R B, and Manickam J 2004 *Comp. Phys. Commun.* **164** 178